Multicomponent imaging with distributed acoustic sensing

Ivan Lim Chen Ning & Paul Sava
Center for Wave Phenomena, Colorado School of Mines

ABSTRACT
The usage of Distributed Acoustic Sensing (DAS) in geophysics is rapidly gaining popularity due to its dense spatial sampling and low operation cost, and given that the optical fiber is easily accessible. In the borehole environment, optical fibers for DAS are often readily available as a part of other sensing tools, such as for temperature and pressure. Although DAS provides single axial strain measurement along the fiber, the entire strain tensor can also be recovered through a combination of purposefully-designed optical fibers. Such reconstruction uses multiple strain projections acquired by manipulating the geometry of the optical fiber. Similarly, using the same approach the reconstruction of the displacement vector is possible. The availability of the entire strain tensor opens the possibility for accurate elastic wavefield extrapolation, thus avoiding the generation of nonphysical wave modes that contaminate migrated images. This technology also enables high-quality estimation of reservoir properties, and accurate elastic parameter estimation.

Key words: seismic acquisition, distributed sensor, optical fiber, multicomponent, imaging

1 INTRODUCTION

DAS acquires strain along an optical fiber coupled to the ground, which represents the projection of the surrounding strain tensor corresponding to the position of the optical fiber. As shown by Lim Chen Ning and Sava (2016), it is possible to reconstruct six components of the strain tensor by using multiple strain projections measured from a combination of a helical and straight optical fibers or a single chirping (variable wrapping angle) helical optical fiber. The working principle of this method requires to exploit consecutive measurements within a given spatial window to perform the strain reconstruction. Although the reconstruction results are promising, the method suffers a drawback from the assumption associated with the spatial window that it should be significantly larger than the seismic wavelength of interest. Implementing this method to short seismic wavelength applications such as microseismic is rather difficult.

Lim Chen Ning and Sava (2017) overcome this limitation by proposing a new configuration that allows the reconstruction of the entire strain tensor without the need to group consecutive measurements. They use a configuration with five equally spaced constant pitch angle helical optical fibers and a straight optical fiber to obtain multiple strain projections that sufficiently describe the surrounding strain tensor for the reconstruction. The pitch angle is measured between the tangent vector and the orthogonal direction of the DAS cable. Using six different strain projections, one can reconstruct the entire strain tensor at a given location. This configuration limits the engineering complexity required to build a multi-fiber cable, thus making such data acquisition feasible. Lim Chen Ning and Sava (2017) reconstruct the strain tensor using the information of the strain projections associated with the geometry of the optical fiber, as well as the gauge length captured in an operator defined by the DAS system. This method, therefore, removes the averaging effect in the reconstruction process, which enables the use of the reconstructed strain data as point measurements.

The stress tensor can be obtained from the reconstructed strain tensor if the material properties surrounding the optical fiber are known or estimated accurately. The stress and displacement data can be used for exact elastic wavefield extrapolation, as shown by Ravasi and Curtis (2013). Conventional methods of elastic wavefield extrapolation using only displacement data (i.e. when stress data are not readily available) are heuristic schemes that do not satisfy the representation theorem. Hence, multicomponent DAS measurements can provide recovery of all information for exact wavefield extrapolation in models of arbitrary complexity. We demonstrate the potential application of multicomponent DAS data with the TTI Marmousi II model adapted from Yan and Sava (2009) and Rocha et al. (2017).

2 METHODOLOGY

In order to obtain the stress data for the wavefield extrapolation, we use the DAS configuration of five equally spaced helical optical fibers and a straight optical fiber proposed by Lim Chen Ning and Sava (2017) to perform the reconstruction of the strain tensor. The equally spaced helical fibers provide sufficient azimuthal sampling of the surrounding strain tensor. However, the reconstruction is only possible with the additional straight optical fiber to constrain the inversion. Upon reconstruction of the strain tensor and assuming an accurate estimation of the Earths surface material properties surrounding the optical fiber, we obtain the stress tensor from the strain tensor through conventional stress-strain relations. As suggested by Lim Chen Ning and Sava (2017), we perform a parameter space search to select our optimal cable configuration using the associated condition number defined from the Gram matrix $\mathbf{L}^\intercal\mathbf{L}$ where the operator $\mathbf{L}$ is a cascade of operators

$$\mathbf{L} = \mathbf{WAG}. \tag{1}$$

$\mathbf{G}$ is the transformation matrix that captures the geometric information of the optical fiber to project the strain tensor onto the optical fiber direction. $\mathbf{A}$ is a band matrix characterizing the gauge length, and $\mathbf{W}$ is a windowing matrix that sets the channel spacing between consecutive average strain measurement within a gauge length. In the proposed multicomponent DAS configuration by Lim Chen Ning and Sava (2017), every row of the operator $\mathbf{L}$ is responsible for an individual measurement of the respective optical fibers. Using measurements $\mathbf{d}$ from the individual optical fibers, we reconstruct the strain tensor $\mathbf{m}$ in a least-squares sense as

$$\mathbf{m} = \left(\mathbf{L}^\intercal\mathbf{L}\right)^{-1}\mathbf{L}^\intercal\mathbf{d}, \tag{2}$$

An example of the parameter space scan is shown in Figure 1(a) where we seek parameter combinations with the lowest condition number. A low condition number implies that the reconstruction of the strain tensor using the associated design parameters is feasible. To narrow the search in the gauge length space, we can set the geometry design parameters such as the diameter at 1 in and the pitch angle at 20°. Since the gauge length is a DAS interrogator parameter, it does not change the configuration geometry. The line in Figure 1(a) represents the defined diameter and pitch angle parameters, and the graph in Figure 2 shows the corresponding condition numbers as a function of gauge lengths. The high condition numbers refers to DAS measurements that do not contain azimuthal information when the gauge length is equal to a multiple of the helix lead which is the axial advance of a helix for a complete 360° turn. This high condition number phenomenon further highlights the need for careful selection of design parameters to ensure accurate strain tensor reconstruction. Figure 3 shows an illustration of the optical fiber configuration using the design parameters marked in Figure 2.

We also can perform similar reconstruction for the three-component displacement vector given that we obtain the displacement projections along the optical fiber through accurate conversion from the native strain projection measurements, such as integration or through relationships presented by Mikumo and Aki (1964); Langston et al. (2006); Langston (2007). Applying the same parameter scanning method suggested by Lim Chen Ning and Sava (2017), we utilize the displacement projection matrix instead of the strain projection matrix. By fixing the same design parameters ranges as for the strain reconstruction, the corresponding condition number plot is shown in Figure 1(b). Unlike the strain tensor where there are six number of unknowns corresponding to the six components, the three-component displacement has a broader range of design parameter combinations for the reconstruction. It is worth noting that the design parameters that are optimal for the strain tensor reconstruction are also optimal for the displacement vector reconstruction. However, the reverse is not true.

Upon obtaining both the stress tensor and the displacement vector, we perform wavefield extrapolation using the surface integral of the representation theorem (Aki and Richards, 2002) by assuming that both stress and displacement on the surface are due to the body force within the volume. This is similar to the formulation shown by Ravasi and Curtis (2013) as

$$\mathbf{V} \approx -\oint_{\partial\Omega} ds\, \left(\underline{\boldsymbol{\sigma}} * \mathbf{G}^{\mathbf{f}} + \mathbf{u} * \mathbf{G}^{\underline{\mathbf{h}}}\right) \cdot \mathbf{n} \tag{3}$$

where $\mathbf{V}$ denotes the extrapolated displacement wavefield, $\underline{\boldsymbol{\sigma}}$ and $\mathbf{u}$ are the measured stress tensor and displacement vector respectively. The wavefield extrapolation uses both the stress tensor data $\underline{\boldsymbol{\sigma}}$ as a dipole source in the wavefield propagator $\mathbf{G}^{\mathbf{f}}$, and the displacement vector $\mathbf{u}$ as a quadrupole source in the wavefield propagator $\mathbf{G}^{\underline{\mathbf{h}}}$. The integral is implied by simultaneously injecting at the surface $\partial\Omega$ which is defined by all the receiver locations. The vector $\mathbf{n}$ is the normal to surface $\partial\Omega$. Conventionally, such extrapolation method is impossible as the stress tensor data are not available. Therefore, in instances where only displacement data are available, we perform the heuristic extrapolation method given as

$$\mathbf{V} \approx -\oint_{\partial\Omega} ds\, \mathbf{u} * \mathbf{G}^{\mathbf{f}} \tag{4}$$

where we propagate the measured displacement vector $\mathbf{u}$ as a dipole source in the wavefield propagator $\mathbf{G}^{\mathbf{f}}$ to obtain the extrapolated displacement wavefield $\mathbf{V}$.

3 NUMERICAL EXAMPLES

Following the method presented by Lim Chen Ning and Sava (2017), we illustrate an example of the 3D strain tensor reconstruction from axial strain measurements using the optical fiber configuration discussed before using synthetic examples of a complex wavefield. The complex wavefields exhibit triplications caused by a velocity model containing a low-velocity Gaussian anomaly, as shown in Figure 4(c). We use smaller than usual gauge lengths such as 0.1 m which are possible using specially designed optical fibers, as indicated by Farhadiroushan et al. (2016). Lim Chen Ning and Sava (2017)

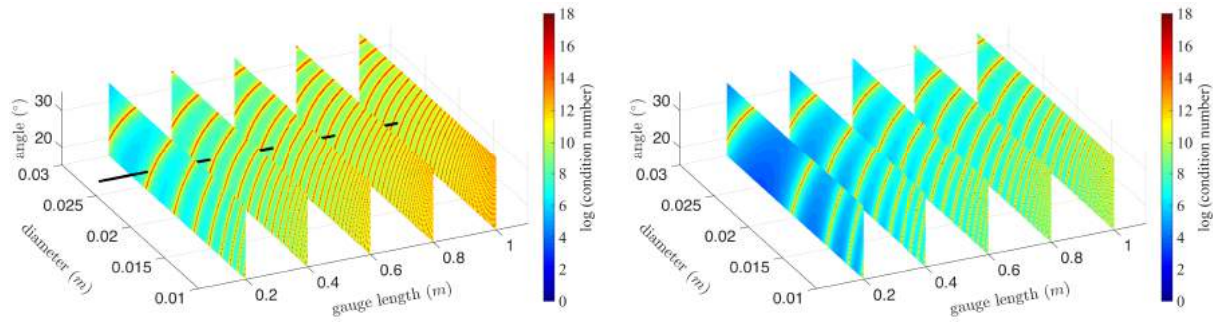

Figure 1. (a) Condition number of the Gram matrix to reconstruct the strain tensor using optical fiber parameters of pitch angle from 15° to 35° and diameter from 0.01 m to 0.03 m. These slices are specifically scanned for but not limited to gauge lengths at every 0.2 m to 1.0 m. (b) Condition number of Gram matrix to reconstruct displacement vectors using the same parameters as (a).

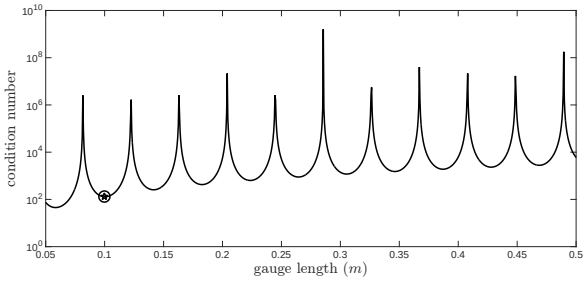

Figure 2. The line in Figure 1(a) is the condition number as a function of gauge lengths with 0.1 m marked.

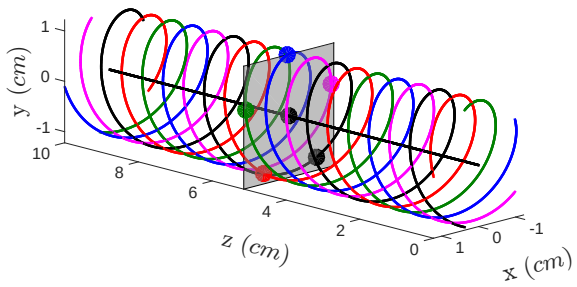

Figure 3. Illustration of five equally spaced helical optical fibers and a straight optical fiber using selected design parameters from Figure 2. The dots represent measurement at the same level along the cable indicated by the horizontal plane.

demonstrate the use of a more conventional fiber system with a gauge length of 1.0 m. The condition numbers for the gauge length of 0.1 m marked in Figure 2 corresponds to a low value.

Our numerical setup mimics a simultaneous source experiment with three sources indicated by the dots and the receivers indicated by a straight line of coordinates (x_b, y_b) in Figure 4(a). Figure 4(b), shown in a tensor layout, represents our target strain reconstruction observed along the receiver location at (x_b, y_b). The horizontal and vertical axes of the individual panels represent the distance along optical fiber and time, respectively. We perform the reconstruction by adding random noise with 10% of the maximum amplitude of the data and in the data frequency band. When the signal is weak, the noise overwhelms the signal. Using a gauge length of 0.1 m, we can reconstruct the strain tensor as shown in Figure 5(a). The difference plot in Figure 5(b) shows no signal leakage and only contain primarily random noise.

In the example using the modified TTI Marmousi II model (Bourgeois et al., 1991; Yan and Sava, 2009; Rocha et al., 2017), we assume the deployment of a multicomponent DAS system to reconstruct the entire strain tensor and the displacement vector. We also assume that the properties of the EarthFLs surface material are known to perform strain to stress conversion. We adopt the energy imaging condition by Rocha et al. (2017) to produce a single elastic image without wave-mode decomposition. Figure 6(a) shows the single shot image obtained through heuristic wavefield extrapolation using displacement data only. The nonphysical waves present themselves as events crosscutting the geological reflectors, especially in the shallow section. The crosscutting is further highlighted in the zoomed section in the shallow region as illustrated in Figure 6(c). However, Figure 6(b) shows an improved single shot image obtained using exact wavefield extrapolation and the corresponding zoomed section in Figure 6(h). The same observation holds for the image obtained by stacking multiple shots. Although the crosscutting in Figure 6(a) appears to be less severe after stacking in Figure 6(e), the geological reflectors are not as coherent when compared to Figure 6(f). The difference between heuristic and exact wavefield extrapolation is better illustrated by the zoom sections in the shallow region of the stacked image in Figure 6(g) and Figure 6(h) respectively. Extrapolating with both stress and displacement eliminates the non-physical waves, thus reducing the uncertainty associated with the crosscutting artifacts in the final image.

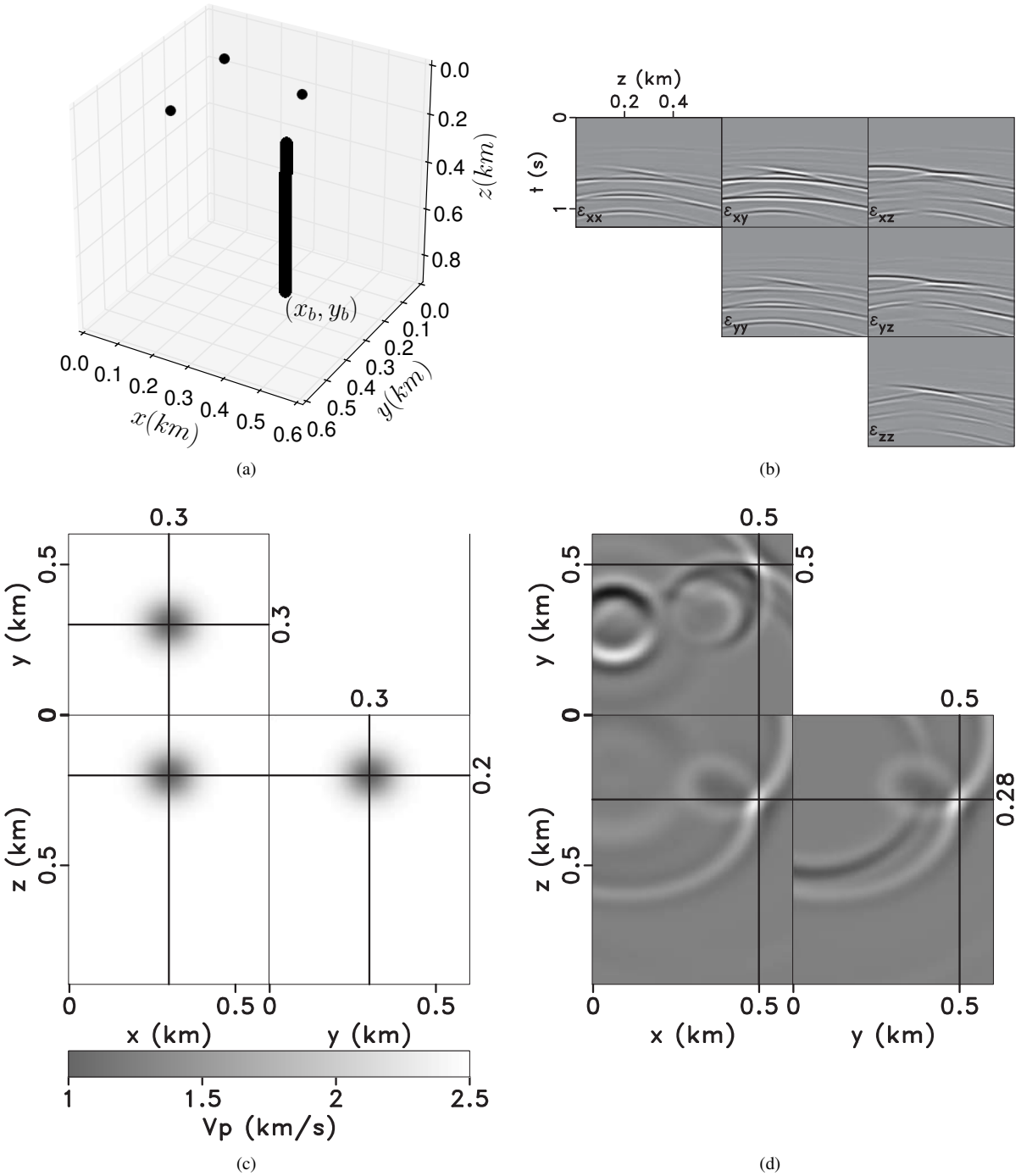

Figure 4. (a) Schematic representation of a DAS experiment depicting the source (dot) and receiver (line) locations. (b) The ideal strain tensor that we would like to reconstruct from DAS measurements. (c) The P-wave velocity model containing a low velocity Gaussian anomaly designed to produce wavefield triplications. The S-wave velocity is half of the P-wave velocity. (d) A snapshot of the vertical displacement wavefield.

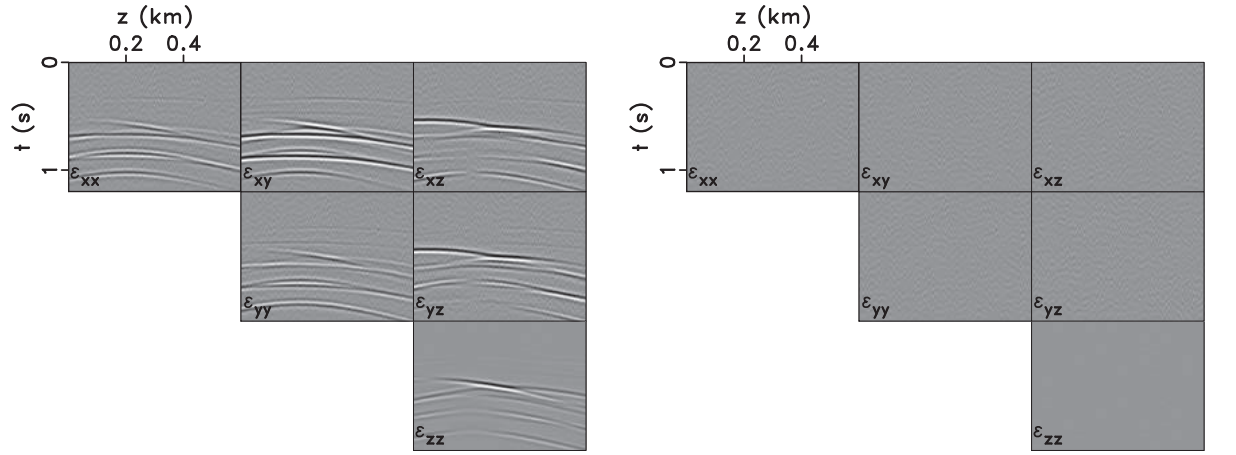

Figure 5. Strain tensor reconstructed from data containing random noise with 10% of the maximum data amplitude and band-limited to the data band with five equally spaced helical optical fibers and a straight optical fiber using a gauge length of (a) 0.1 m. Panel (b) is the difference between the ideal strain tensor in Figure 4(b) and the reconstructed tensor in (a).

4 CONCLUSION

We demonstrate the possibility of accurate reconstruction of the strain tensor using distributed acoustic sensing data by measuring strain projections along several optical fibers opens the possibility for accurate elastic wavefield extrapolation. This requires optical fiber system that is purposefully built to access diverse projections of the strain tensor. The design parameters mentioned in this paper serve as an example of how one parameterizes a multicomponent DAS acquisition system with five equally spaced helical optical fibers, together with a straight optical fiber. From our analysis, a shorter gauge length plays a significant role in the accuracy of the strain tensor reconstruction in the presence of noise. Systems with short gauge length are possible with specially-engineered optical fiber together with rapidly evolving DAS interrogator technology. Even using current technology, increasing the diameter of our multi fiber configuration when the dimension of the fiber is not restricted, such as for surface seismic acquisition, allows the use of larger gauge lengths. However, as seen in our analysis, careful selection of the design parameters through parameter scanning is necessary to ensure accurate reconstruction. The more accurate wavefields lead to a higher quality image without the presence of nonphysical waves in the elastic medium, which supports reservoir characterization in complex geological structures. The technique discussed in this paper applies to elastic models characterized by arbitrary anisotropy and heterogeneity.

5 ACKNOWLEDGMENTS

We would like to thank the sponsors of the Center for Wave Phenomena, whose support made this research possible and Martin Karrenbach of OptaSense for fruitful discussions. The reproducible numeric examples in this paper use the Madagascar open-source software package (Fomel et al., 2013) freely available from http://www.ahay.org.

REFERENCES

Aki, K., and P. G. Richards, 2002, Quantitative seismology.

Bourgeois, A., M. Bourget, P. Lailly, M. Poulet, P. Ricarte, and R. Versteeg, 1991, Marmousi, model and data: Presented at the 1990 EAGE workshop on Practical Aspects of Seismic Data Inversion.

Farhadiroushan, M., T. Parker, and S. Shatalin, 2016, Method and apparatus for optical sensing: WO Patent App. PCT/GB2016/050, 625.

Fomel, S., P. Sava, I. Vlad, Y. Liu, and V. Bashkardin, 2013, Madagascar: open-source software project for multidimensional data analysis and reproducible computational experiments: Journal of Open Research Software, **1**.

Langston, C. A., 2007, Spatial gradient analysis for linear seismic arrays: Bulletin of the Seismological Society of America, **97**, 265–280.

Langston, C. A., P. Bodin, C. Powell, M. Withers, S. Horton, and W. Mooney, 2006, Explosion source strong ground motions in the Mississippi embayment: Bulletin of the Seismological Society of America, **96**, 1038–1054.

Lim Chen Ning, I., and P. Sava, 2016, Multicomponent distributed acoustic sensing: 86th Annual International Meeting, SEG, Expanded Abstracts, 5597–5602.

———, 2017, High-resolution multicomponent distributed acoustic sensing: 87th Annual International Meeting, SEG, Expanded Abstracts, 941–946.

Mikumo, T., and K. Aki, 1964, Determination of local phase velocity by intercomparison of seismograms from strain and pendulum instruments: Journal of Geophysical Research, **69**, 721–731.

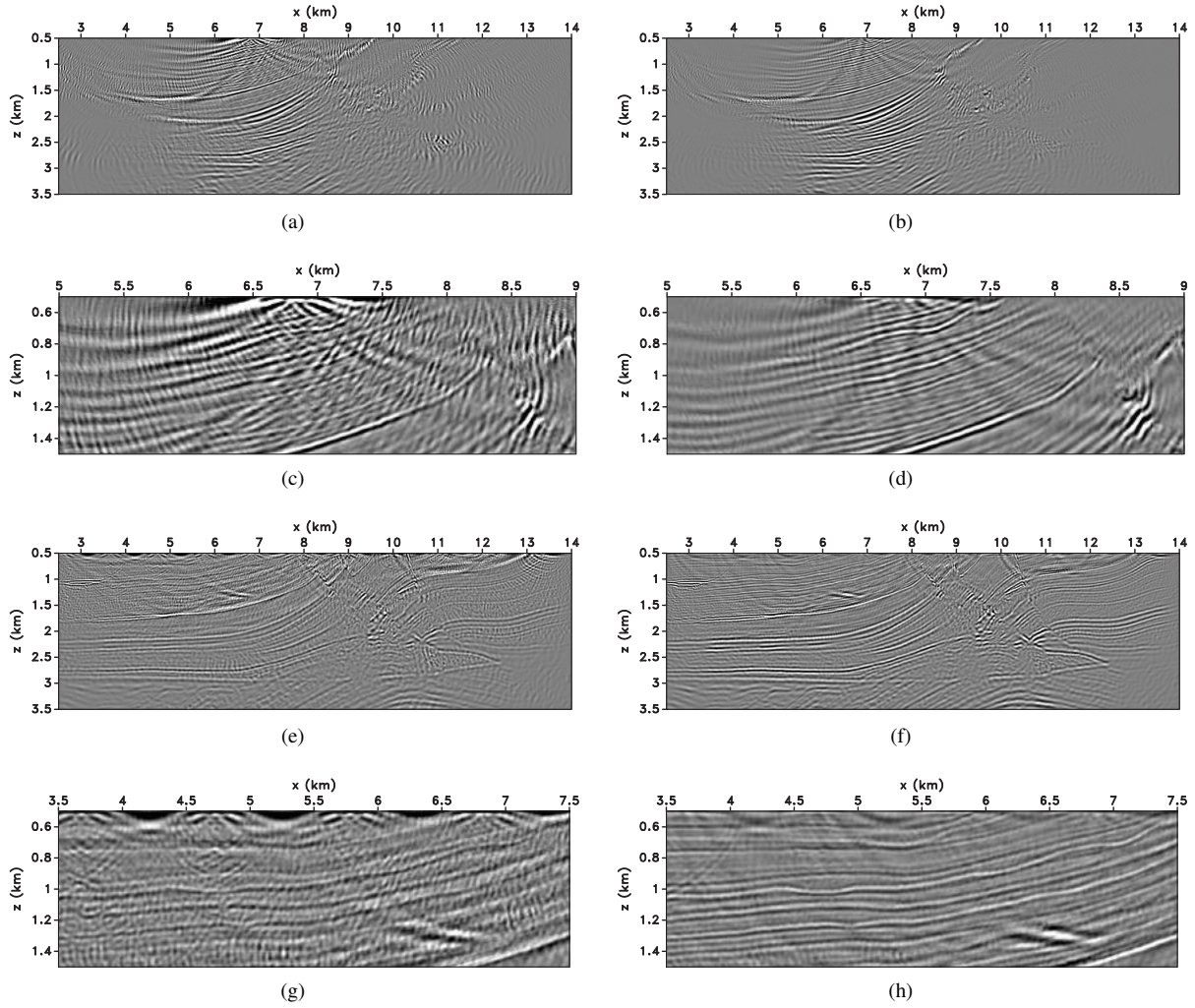

Figure 6. Images obtained using the energy imaging condition from the Marmousi II experiment: (a) **single shot** image using the exact and (b) heuristic wavefield extrapolation. The energy image in panel (c) and (d) is the zoom section of the respective panels in (a) and (b). The **stacked** images in panel use (e) the exact and (f) heuristic wavefield extrapolation. The respective zoom energy image for panel (e) and (f) is shown in (g) and (h).

Ravasi, M., and A. Curtis, 2013, Elastic imaging with exact wavefield extrapolation for application to ocean-bottom 4C seismic data: Geophysics, **78**, S265–S284.

Rocha, D., N. Tanushev, and P. Sava, 2017, Anisotropic elastic wavefield imaging using the energy norm: Geophysics.

Yan, J., and P. Sava, 2009, Elastic wave-mode separation for VTI media: Geophysics.